INCORPORATION OF ATMOSPHERIC FLOW FIELDS AND GROUND INTERACTIONS INTO ACOUSTIC FINITE-DIFFERENCE, TIME-DOMAIN SIMULATIONS

D. Keith Wilson*
U.S. Army Cold Regions Research and Engineering Laboratory
Hanover, NH 03755

David H. Marlin
U.S. Army Research Laboratory
White Sands Missile Range, NM 88002

Sandra L. Collier
U.S. Army Research Laboratory
Adelphi, MD 20783

Neill P. Symons, David F. Aldridge
Sandia National Laboratories
Albuquerque, NM 87185

Vladimir E. Ostashev
NOAA Environmental Technology Laboratory
Boulder, CO 80305

ABSTRACT

By providing highly realistic simulations of sound propagation through complex atmospheric and terrain environments, finite-difference time-domain (FDTD) techniques can potentially reduce development time and improve the battlefield performance of acoustic sensors. In this paper, we summarize recent progress in improving two key aspects of acoustic FDTD calculations for the atmosphere: (1) development of a rigorous implementation of sound propagation in a moving, inhomogeneous fluid, and (2) formulation and numerical implementation of time-domain methods for handling sound interactions with partially reflecting ground surfaces. The new techniques are illustrated with highly detailed calculations of sound propagation through simulated, dynamic atmospheric turbulence fields and over a porous ground surface with viscous and thermal relaxation mechanisms.

1. INTRODUCTION

Acoustic sensors are expected to play a key role in the Army's Future Force by providing rapidly deployable, networked surveillance over wide areas. It is well known that the performance of acoustic sensors is affected by complex sound propagation phenomena occurring in outdoor settings, such as reflections from trees and buildings, ground interactions, scattering by turbulence, refraction by wind and temperature gradients, and diffraction over hills. The expense and difficulty of performing comprehensive, controlled field experiments outdoors, combined with the rapid schedule for fielding the Future Force, makes necessary novel approaches to advanced sensor development. A realistic simulation of complex environmental effects on propagating sound, when combined with detailed source signature and high-resolution atmospheric and terrain inputs, could be immensely valuable in shortening the requirements-to-deployment cycle for acoustic sensors, developing robust signal information processing stategies, and improving sensor utilization doctrine.

Most current numerical methods for outdoor sound propagation, such as the fast field program and parabolic equation (Salomons, 2001), are incapable of, or poorly suited to, simulating all of the propagation phenomena mentioned in the preceeding paragraph. Complex, moving source distributions, such as maneuvering ground vehicles, are also difficult to incorporate. These shortcomings can potentially be overcome with finite-difference, time-domain (FDTD) techniques, which have become popular for electromagnetic and seismic wave propagation. But there are significant drawbacks to FDTD techniques that have so far prevented their widespread use for outdoor sound propagation. Foremost among these is that they are very computationally intensive when applied to the frequency range (a few hundred Hz and lower) and spatial scales (a few km or less) of Army tactical applications for acoustic sensors. Fortunately, the current generation of parallel-processing computers now makes FDTD calculations viable. Some other difficulties, particular with the sound propagation problem, are (1) incorporating the dynamically moving (windy and turbulent) atmospheric propagation medium, and (2) formulating time-domain techniques for the acoustic interactions with the ground, including absorption and dispersion characteristics of porous materials such as soils. Successfully addressing these two problems is key to making acoustic FDTD simulation useful for Army

Report Documentation Page

Form Approved
OMB No. 0704-0188

1. REPORT DATE	2. REPORT TYPE	3. DATES COVERED
00 DEC 2004	**N/A**	**-**

4. TITLE AND SUBTITLE	5a. CONTRACT NUMBER
Incorporation Of Atmospheric Flow Fields And Ground Interactions Into Acoustic Finite-Difference, Time-Domain Simulations	5b. GRANT NUMBER
	5c. PROGRAM ELEMENT NUMBER
6. AUTHOR(S)	5d. PROJECT NUMBER
	5e. TASK NUMBER
	5f. WORK UNIT NUMBER
7. PERFORMING ORGANIZATION NAME(S) AND ADDRESS(ES) **U.S. Army Cold Regions Research and Engineering Laboratory Hanover, NH 03755; U.S. Army Research Laboratory White Sands Missile Range, NM 88002**	8. PERFORMING ORGANIZATION REPORT NUMBER
9. SPONSORING/MONITORING AGENCY NAME(S) AND ADDRESS(ES)	10. SPONSOR/MONITOR'S ACRONYM(S)
	11. SPONSOR/MONITOR'S REPORT NUMBER(S)

12. DISTRIBUTION/AVAILABILITY STATEMENT
Approved for public release, distribution unlimited

13. SUPPLEMENTARY NOTES
See also ADM001736, Proceedings for the Army Science Conference (24th) Held on 29 November - 2 December 2005 in Orlando, Florida. , The original document contains color images.

14. ABSTRACT

15. SUBJECT TERMS

16. SECURITY CLASSIFICATION OF:			17. LIMITATION OF ABSTRACT	18. NUMBER OF PAGES	19a. NAME OF RESPONSIBLE PERSON
a. REPORT	b. ABSTRACT	c. THIS PAGE			
unclassified	**unclassified**	**unclassified**	**UU**	**8**	

Standard Form 298 (Rev. 8-98)
Prescribed by ANSI Std Z39-18

applications. These problems are the focus of this paper.

Incorporation of a dynamically moving atmosphere is discussed in Section 2. There the time-domain differential equations needed to propagate the sound fields through a propagation medium in motion are described and some of the numerical issues involved in their implementation are addressed. An example is provided with inputs to an FDTD calculation provided by an atmospheric large-eddy simulation (LES). Section 3 describes acoustic interactions with porous materials such as the ground and their implementation in time-domain calculations. Due to the historical emphasis in acoustics on frequency-domain computational methods, our time-domain analysis represents a fundamentally new approach.

2. ACOUSTIC FDTD CALCULATIONS IN A MOVING MEDIUM

For most terrestrial problems involving electromagnetics or seismics, the propagation medium (atmosphere or Earth) does not move or otherwise change significantly as waves propagate between sources and receivers of interest.[1] The same cannot be said, however, for sound propagation through the atmosphere. Propagation times and atmospheric variations both occur in seconds or less for most scenarios of tactical interest to the Army. Wind Mach numbers (the ratio of the wind speed to the sound speed) are commonly as high as 1/50 in the near-Earth atmosphere and 1/5 in a stratospheric jet stream. To be useful in Army applications, numerical methods for sound propagation in the atmosphere must account for the effects of wind, turbulence, and other atmospheric disturbances.

In this section, we consider various aspects of including a moving propagation medium in acoustic FDTD calculations. An accurate treatment has required derivation of a new set of coupled state equations, together with numerical methods for solving it.

2.1 Coupled Equation Set

The wave equation, which is the starting point for most sound propagation calculations, is a second-order partial differential equation in both time and space. FDTD techniques, however, are most readily applied to first-order partial differential equations (that is, a state equation set). Furthermore, most solutions of the wave equation have been based on one-way approximations, in which the energy is propagated in only one direction, and on effective sound-speed approximations, in which the sound speed is taken to be the actual sound speed plus the component of the wind velocity in the direction of propagation. Wave equations in a moving medium that do not use these approximations are considerably more complicated than the wave equation for a stationary medium (Ostashev, 1997). Fortunately, the switch to first-order equations facilitates correct handling of the wind velocity field. The following coupled, first-order equations for the acoustic pressure p and acoustic particle velocity $\mathbf{w}$ involve no one-way or effective sound-speed approximations, and therefore provide an appropriate starting point for accurate FDTD calculations in a moving atmosphere (Ostashev et al., 2004):

$$\frac{\partial p}{\partial t} = -\left(\mathbf{v}\cdot\nabla\right)p - \rho c^2 \nabla\cdot\mathbf{w} + \rho c^2 Q, \tag{1}$$

$$\frac{\partial \mathbf{w}}{\partial t} = -\left(\mathbf{w}\cdot\nabla\right)\mathbf{v} - \left(\mathbf{v}\cdot\nabla\right)\mathbf{w} - \frac{\nabla p}{\rho} + \frac{\mathbf{F}}{\rho}. \tag{2}$$

Here, ρ is medium density, c is the adiabatic speed of sound, and $\mathbf{v}$ is the wind velocity. The quantities $\mathbf{F}$ and Q represent sources: the former is a force acting on the medium, whereas the latter is a mass source. Bold symbols represent vectors. The terms involving $(\mathbf{v}\cdot\nabla)$, which are particular to the moving medium, are called the *advective* terms. Numerical issues aside, the source terms and atmospheric field variables can be arbitrary functions of space and time.

Equations (1) and (2) were derived in Ostashev et al. (2004) from the full fluid dynamical equations using the conventional linear acoustics approximation, namely that the sound wave is a small perturbation to the background state of the medium. Additionally, the sound waves are assumed to be uninfluenced by the following: (1) divergence in the atmospheric flow, (2) the background pressure gradient, and (3) the Coriolis force. The first of these implies that turbulent fluctuations in the flow have a low Mach number, which is very reasonable for the problems considered here. The second may be considered a distinguishing property between sound and gravity waves. The third is valid for even for very low infrasonic frequencies. An FDTD code based on Eqs. (1) and (2) is both more general and accurate than most current sound propagation formulations, despite its comparative simplicity.

2.2 Computational Considerations

Typically, finite-difference solutions for wave propagation in a *nonmoving* medium use a grid that is staggered in space and time (Botteldooren, 1994; Graves, 1996). Each acoustic particle velocity component is explicitly calculated on spatial grid nodes shifted by one-half of the internode spacing, relative to the explicit acoustic pressure nodes, in the direction of the velocity component. The particle velocities and pressures are advanced on alternating time steps. The finite-difference stencil corresponding to the pressure advancement in this approach is illustrated in Figure 1. It happens, however, that this staggered "leap-frog" methodology of alternately marching the solution in time cannot be applied directly to Eqs. (1) and (2). Evaluation of the advective terms on the right-hand sides of these equations requires knowledge of the pressure and particle velocity fields at time steps where they are not explicitly available. Therefore, we have developed alternative approaches based on unstaggered temporal grids (Ostashev et al., 2004; Wilson and Liu, 2004) and staggered temporal grids spanning multiple time steps (Symons et al., 2003). (In either case, a staggered spatial grid is still used.) The latter, staggered approach is shown schematically in Figure 2. This finite-difference stencil provides fully centered spatial finite differences in the context of the moving medium problem. As discussed in Wilson and Liu (2004), this approach and

[1] There are some notable exceptions to this statement, such as Doppler shifts in signals from clear-air radars.

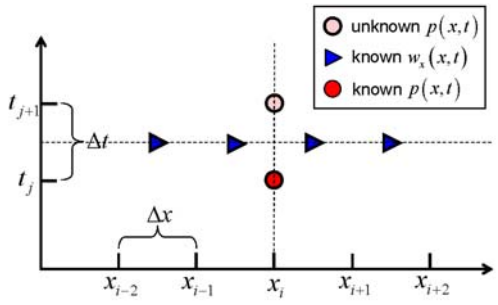

FIG. 1: Standard O(4,2) (fourth order in space, second order in time) staggered leap-frog finite-diference stencil for updating the acoustic pressure solution in a non-moving medium. For simplicity, the stencil is shown with only one spatial dimension. Time is the vertical axis and space is horizontal, with corresponding grid intervals Δt and Δx, respectively. The dashed lines intersect at the pivot point, which is the location on which the finite-difference approximations are centered.

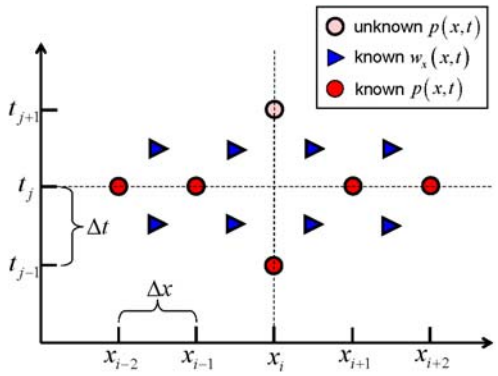

FIG. 2: New O(4,2) staggered finite-diference stencil for updating the acoustic pressure solution in a moving medium. Two time levels must be stored in comparison to the single time level for the non-moving medium.

several others can yield highly accurate results, although some efficiency in memory usage and/or calculation time is lost in comparison to the customary leap-frog solution for a nonmoving medium.

The size and dimensions of the computational domain in an acoustic FDTD simulation depend on the propagation geometry of interest and the memory available. Artificial sound absorbing layers are usually placed around the sides and corners of the domain to prevent unwanted numerical reflections. The lower surface is normally taken as a rigid plate, although more sophisticated and realistic partially absorbing ground models are under development as described in Section 3. The spacing between grid points in acoustic is driven by the smallest acoustic wavelength of interest. For fourth-order spatial finite differencing, a typical grid spacing would be 1/8 of the wavelength. To illustrate the memory requirements, consider a simulation in which a source emits frequencies at 250 Hz and lower. For a sound speed of 340 $\mathrm{m\,s^{-1}}$, the minimum wavelength is $340/250 = 1.36$ m, and the spatial grid interval therefore 0.17 m. Assuming the dimensions of the computational domain are 500 m in each horizontal direction and 50 m in the vertical, about 2.5×10^9 grid nodes are required. Such intensive computational problems can be tackled only on very large, parallel processing computers.

2.3 High Mach Number Tests of the Solution Technique

We now consider 2D FDTD calculations for the case of a stationary source in a uniform, high Mach number wind. Although this is a simple case, it is very useful for testing the fidelity of the numerical solution method, since an analytical solution is known. For this series of calculations, a mass-type source was used that consisted of a 10-cycle, 100-Hz signal with a cosine taper function applied to the three periods at the beginning and end. The tapering alleviates numerical dispersion of high frequencies, which can become evident when there is an abrupt change in the source emission.

Figure 3 illustrates the pressure field calculation for a uniform Mach 0.3 wind. The field is shown at 0.11 s, or 0.01 s after the source has been turned off. Note that the distance between wave fronts is smaller upwind than downwind, due to the role of the wind in determining the overall propagation speed. Although not as clearly evident, the pressure amplitude is higher upwind than downwind. The azimuthal dependence of $|p(r, \alpha, M)/p(r, 0, 0)|$ at a distance $r = (10/\pi)\,\lambda$ (where λ is the wavelength, α the azimuthal angle measured from upwind, and M is the Mach number) is plotted and compared to the theoretical prediction in Figure 4 for $M = 0$, 0.3, and 0.6. Two calculated curves for each value of M are shown, one for a low-resolution run with 800×800 grid points and a time step $\Delta t = 0.145$ ms, and the other for a high-resolution run with 1600×1600 grid points and $\Delta t = 0.0362$ ms. For $M = 0.3$, both grid resolutions yield nearly exact agreement with theory. Agreement with theory at $M = 0.6$ is very good for the high-resolution run, although the low-resolution run substantially underpredicts the upwind amplitude. High spatial resolution is needed at high Mach numbers because of the shortening of the wavelength in the upwind direction.

2.4 Simulations with Dynamic Atmospheric Models

The time-domain nature of acoustic FDTD simulation makes it a natural approach for coupling with dynamic atmospheric models such as global and mesoscale numerical weather predictions (NWP) and large-eddy simulations (LES) of the atmospheric boundary-layer (ABL) and flow in urban terrains. In this section, we present examples of FDTD simulations of sound propagating through ABL turbulence fields generated by LES. The LES we use is a parallelized implementation of the physical models and code described in Sullivan et al. (1994). Two stability cases are considered. The first is for a neutral ABL (Figure 5)

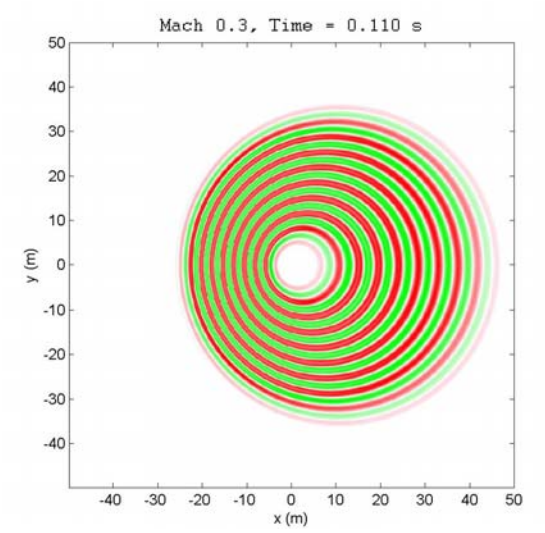

FIG. 3: Wavefronts of the sound pressure due to a 100-Hz point source located at $x = 0$ and $y = 0$. A uniform flow with Mach number 0.3 moves from left to right.

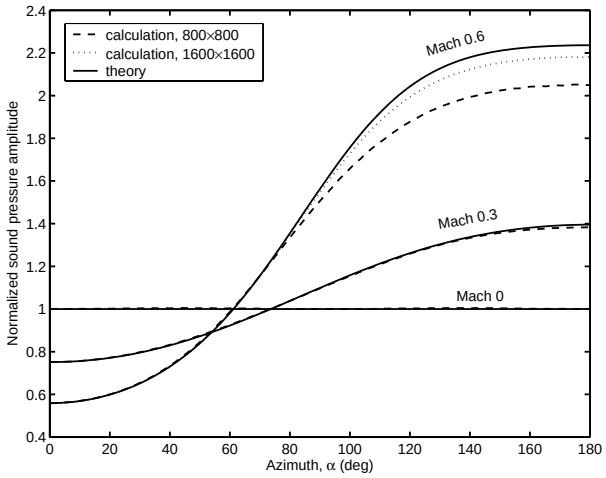

FIG. 4: Comparison of the angular dependence of the pressure amplitude from FDTD calculations to theory. The downwind direction is 0° and the upwind direction is 180°. Calculations for grids at two different resolutions and three different Mach numbers are shown.

and the second for a buoyantly unstable ABL (Figure 6). Although only the vertical velocity component is shown in these figures, all three velocity components and temperature were used as input to the acoustic FDTD calculation. The sound speed c in Eqs. (1) and (2) is known from the absolute temperature T according to the relationships $c = 20.02\sqrt{T}$; the density follows from the ideal gas law.

The acoustic calculation was performed in 3D with $901 \times 901 \times 603$ grid nodes spaced at 1 m. The time step was 0.25 ms and the solution was advanced over 16001 time steps. The sound source was a 20-Hz, mono-frequency, mass-type source. Execution required 10 hours on a cluster built from 100 Compaq ES45 processors, making this run likely the single most computationally intensive and detailed calculation of sound propagation in the ABL yet performed.

The middle panels in Figures 5 and 6 show snapshots of the calculated sound fields. Distortions to the propagating wavefronts are not easily discernable in these images as presented. For each case we also propagated sound fields through horizontally averaged LES fields (i.e., the mean vertical profiles only). The difference between the sound fields, with and without the horizontal LES variability, is shown in the lower panels of Figures 5 and 6. The distortions to wavefront shape and amplitude are easily discernable in these difference images. Such distortions cause fluctuations in apparent bearings of targets derived from acoustic sensor arrays and are the limiting factor in array performance when the signal-to-noise ratio is high. The capability to realistically simulate turbulence effects enables virtual testing of acoustic beamforming systems being developed for the Army's Future Force.

3. TIME-DOMAIN MODELING OF AN ABSORPTIVE GROUND

Typically, in frequency-domain acoustic calculations, the ground interaction is characterized using a localized impedance function Z, defined as

$$Z(\omega) = \frac{P(z=0,\omega)}{W_n(z=0,\omega)},$$

in which P and W_n are the Fourier transforms of the pressure and particle velocity normal to the boundary, respectively, $z = 0$ is the position of the boundary, $\omega = 2\pi f$, and f is the frequency. In this formulation, the acoustic pressure is analogous to voltage in an electrical system, while the particle velocity is analogous to current. The linear ground boundary condition between the pressure and particle velocity generally makes frequency-domain handling of the ground interaction a simple task.

Alternatively, one might explicitly calculate the wave propagation in the ground as well as in the air. In that case, the normal methodology is to use complex operators (frequency-dependent values with real and imaginary parts) to represent the bulk material properties, specifically the density and bulk modulus within the ground. The imaginary parts of the operators relate to wave attenuation and dispersion in the medium. Implementation of complex-valued material properties in most computer programming languages is little more difficult than real-valued material properties.

The impedance ground boundary condition and bulk material methods each have their own relative merits. The former is highly computationally efficient: the wavefield in the ground does not need to be calculated or stored. On the other hand, the bulk material method is called for when one is interested in the waves in the ground or they must be explicitly calculated due to reflections from non-uniform ground properties, such as when a thin layer of soil overlies rock. The bulk material method is also easier to apply

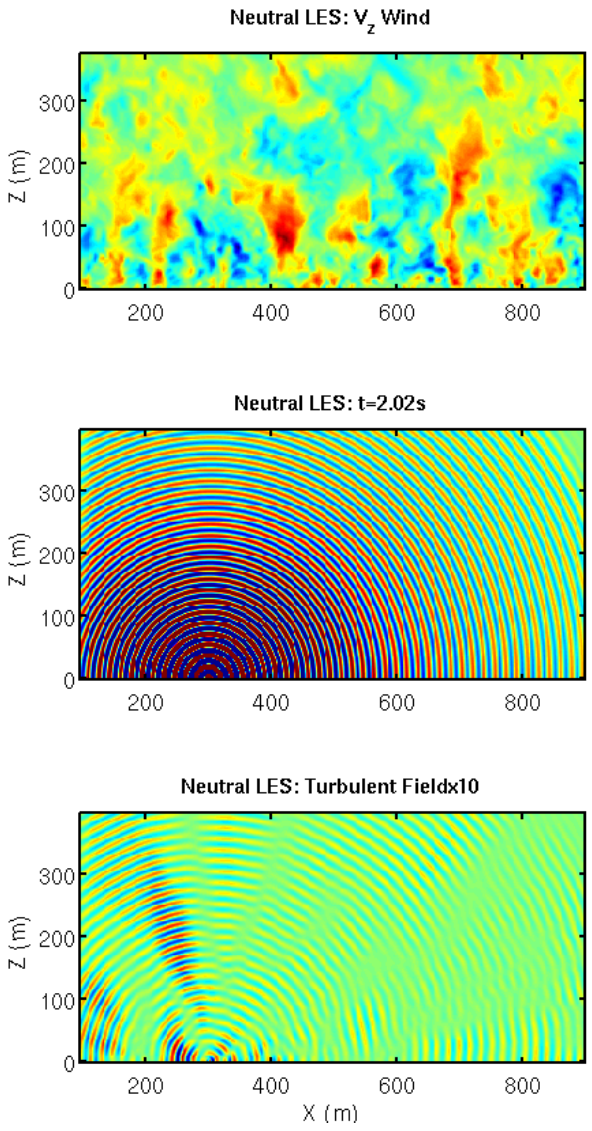

FIG. 5: Top: Vertical wind field from an LES for a neutral ABL ($z_i/L_o = -\infty$). Only a partial cross section of the full LES is shown. The turbulent structures are generated primarily by wind shear. Middle: Acoustic FDTD calculation of waves from a constant-frequency source propagating through the neutral LES fields. Bottom: Difference field, multiplied by 10, between sound field calculated with turbulence (LES fields) and without turbulence (horizontally averaged LES fields).

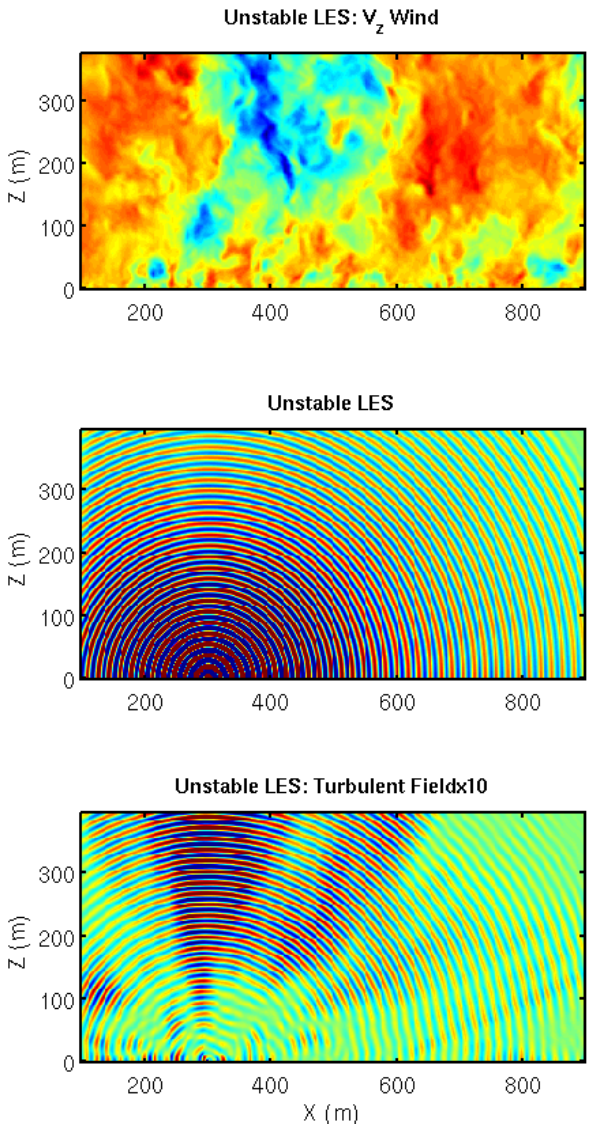

FIG. 6: Same as Figure 5, except for a buoyantly unstable ABL ($z_i/L_o = -6$).

when the surface is not parallel to one of the coordinate directions.

Regardless of whether a ground boundary condition or bulk material approach is appropriate, time-domain procedures for handling attenuation and dispersion in a porous ground material are not nearly so well established as the frequency-domain procedures. Fundamentally, the issue is the reaction time of the porous material, which requires the history of the signal to be stored over an interval of time. If this interval is long compared to the computational time step, a substantial amount of computer memory may be required. In the remainder of this section, we describe approaches to time-domain modeling of the ground, based both on the bulk material and impedance ground boundary condition methods.

3.1 Bulk Material Method

Although dozens of frequency-domain models have been developed for sound propagation in porous materials, we have found that one based on explicitly modeling the viscous and thermal diffusion in the pores as relaxation processes (Wilson, 1993) translates most naturally to the time domain. Other approaches that have been exam-

ined are either non-causal (Berthelot, 2001) or limited in their frequency range of applicability (Zwikker and Kosten, 1949; Fellah and Depollier, 2000), and in any case do not have closed-form analytical solutions in the time domain. A new set of integro-differential equations (Wilson et al., 2004) to be discussed in this section remedies all of these shortcomings with no appreciable loss in accuracy.

The physics underlying the relaxation model can be understood in a straight-forward manner. When a pressure gradient is introduced across a porous material (by a sound wave or other mechanism), air is accelerated through the pores. The acceleration is counteracted by viscous drag forces exerted by the solid frame material. The air flow gradually relaxes to a steady state in which the pressure gradient and viscous forces balance. Similarly, if the air in the pores is heated or cooled, the temperature in the pores gradually relaxes to a thermal equilibrium with the frame material as heat is conducted between the solid and air.[2]

The new set of integro-differential equations (Wilson et al., 2004) describing these processes in the time domain is:

$$\frac{\mathbf{w}}{\tau_\mathrm{v}} + \frac{\partial \mathbf{w}}{\partial t} + \frac{1}{\sqrt{\pi \tau_\mathrm{v}}} \int_{-\infty}^{t} \frac{\mathbf{w}\left(t'\right)/\tau_\mathrm{v} + \partial \mathbf{w}\left(t'\right)/\partial t'}{\sqrt{t-t'}} \times \exp\left(-\frac{t-t'}{\tau_\mathrm{v}}\right) dt' = -V_\infty \nabla p, \quad (3)$$

and

$$\beta_\infty \frac{\partial p}{\partial t} + \frac{\beta_\infty \left(\gamma - 1\right)}{\sqrt{\pi \tau_\mathrm{e}}} \int_{-\infty}^{t} \frac{\partial p\left(t'\right)/\partial t'}{\sqrt{t-t'}} \times \exp\left(-\frac{t-t'}{\tau_\mathrm{e}}\right) dt' = -\nabla \cdot \mathbf{w}. \quad (4)$$

Here, τ_v is the time constant for the viscous relaxation process and τ_e for the thermal (entropy) relaxation process. Additional symbols are: $V_\infty = \Omega/\rho q^2$, the effective specific volume at high frequency, $\beta_\infty = \Omega/P\gamma$, the effective (adiabatic) compressibility at high frequency, Ω, the porosity (void fraction), q, the tortuosity (a measure of the obliqueness of the pores), P, the ambient air pressure, and γ, the ratio of specific heats for air.

The integrals in Eqs. (3) and (4) represent convolutions of the propagating wavefield with the relaxational response function $s\left(t\right) = 1/\sqrt{\pi\tau t}\exp\left(-t/\tau\right)H\left(t\right)$ [where $H\left(t\right)$ is the Heaviside function equal to 0 for $t < 0$ and 1 for $t \geq 0$]. When the relaxation time is very short in comparison to any changes in the propagating wavefield, the response functions can be approximated as unit impulses and the following much simpler set of equations is obtained:

$$\frac{2}{\tau_\mathrm{v}}\mathbf{w} + \frac{3}{2}\frac{\partial \mathbf{w}}{\partial t} = -V_\infty \nabla p, \quad (5)$$

and

$$\beta_\infty \gamma \frac{\partial p}{\partial t} = -\nabla \cdot \mathbf{w}. \quad (6)$$

[2] Typically, the heat capacity of the frame material is so large compared to the air that the frame essentially remains at a fixed termperature while the temperature of the air in the pores attempts to attain equilibrium.

The first of these equations describes a simple balance among viscous, inertial, and pressure gradient forces, whereas the second implies that the propagation is isothermal (that is, the acoustic period is long enough that the temperature in the pores stays in equilibrium with the frame material). With notational changes, these equations are the same as a well known set of phenomenological equations suggested by Zwikker and Kosten (1949) that has more recently been used for acoustic FDTD calculations (Salomons et al., 2002).

As discussed in Section 2.2, in FDTD simulation the wavefield variables are calculated at discrete time steps. The wavefield variables should vary only a small amount between the time steps. Using this assumption, but avoiding any additional ones pertaining to the relative values of the time step and relaxation times, we can readily evaluate the integrals in Eqs. (3) and (4) in a closed form involving error functions. Although the details are not given here, we have succeeded in deriving such a solution and implementing it in a 2D FDTD code.

An example calculation involving a porous ground surface is shown Figures 7–10. The domain is configured with a source in the center, a rigid barrier 20 m to the right of the source, a 20-m thick porous ground layer at the bottom of the domain, and a 20-m thick artificial absorbing layer at the top. The porous material parameters for the ground are $\sigma = 1000$ Pa·s·m^{-2}, $q = 1.8$, and $\Omega = 0.5$, which are reasonable for an "acoustically soft" ground such as snow or coarse gravel. The source in the simulation emits 10 cycles of a 100-Hz sine wave, as described in Section 2.2. No wind flow is present in this calculation.

In Figure 7, corresponding to 0.058 s after source initiation, the sound waves are just beginning to impinge on the barrier. By the time of the second snapshot (Figure 8, taken at 0.116 s) the wavetrain is just starting to penetrate the ground. A diffracted wave curls over the right side of the barrier and a reflection is evident to the right. At 0.151 s (Figure 9), the reflection off the barrier is fully formed and a partial reflection from the ground is also becoming evident. The sound in the ground has a shorter wavelength than in the air and is rapidly attenuated. In Figure 10, taken at 0.250 s, the initial wave and barrier reflection are distinct and propagating leftward, while the barrier diffraction propagates to the right. Weak ground reflections associated with the initial wave and barrier reflection are also visible. Waves in the ground refract strongly toward the surface normal, as is consistent with Snell's law.

3.2 Ground Boundary Condition Method

As mentioned earlier, a ground-boundary condition formulation can provide a substantial savings in computational memory and processing time because the wavefield need not be explicitly calculated in the ground. Based on the viscous and thermal relaxation concept, Wilson (1993) previously derived a full-frequency equation for the impedance of a porous ground surface:

$$Z\left(\omega\right) = \frac{\rho c q}{\Omega}\left[\left(1 + \frac{\gamma - 1}{\sqrt{1 - i\omega\tau_\mathrm{e}}}\right)\left(1 - \frac{1}{\sqrt{1 - i\omega\tau_\mathrm{v}}}\right)\right]^{-1/2}. \quad (7)$$

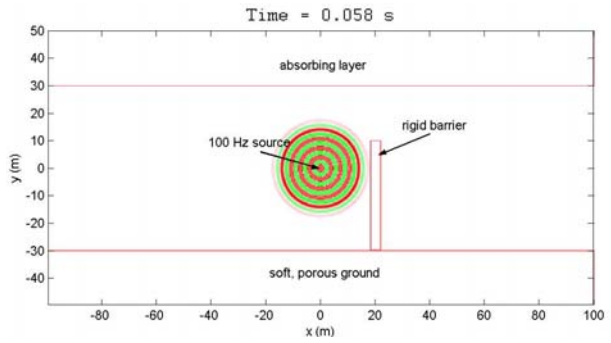

FIG. 7: Propagation above a soft porous ground in the presence of a rigid barrier, 0.058 s after source initiation. The 100-Hz source is located at the middle of the domain, and an absorbing layer is present at the top to eliminate numerical reflections.

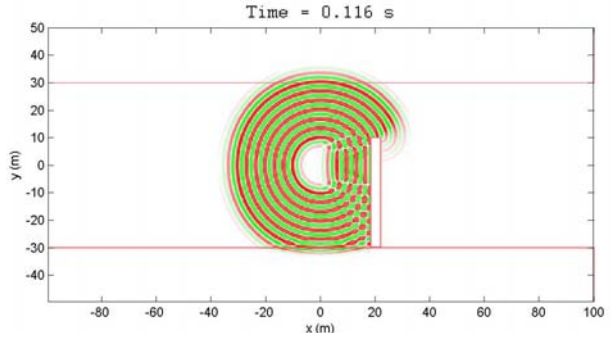

FIG. 8: Propagation above a soft porous ground in the presence of a rigid barrier, 0.116 s after source initiation.

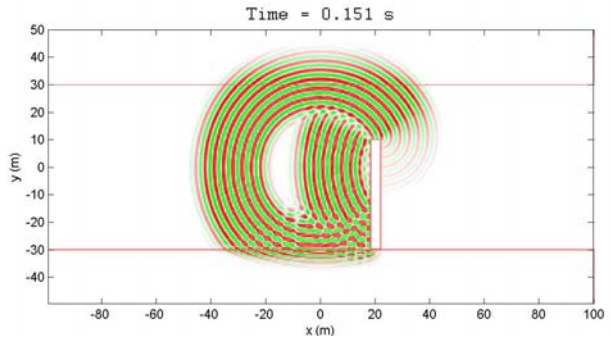

FIG. 9: Propagation above a soft porous ground in the presence of a rigid barrier, 0.151 s after source initiation.

In principle, an inverse Fourier transform could be applied to this equation to determine a time-domain ground boundary condition. However, a closed-form inverse transformation is not known. Fortunately, we have found that the following much simpler equation, derived from a factorization of (7), behaves nearly identically:

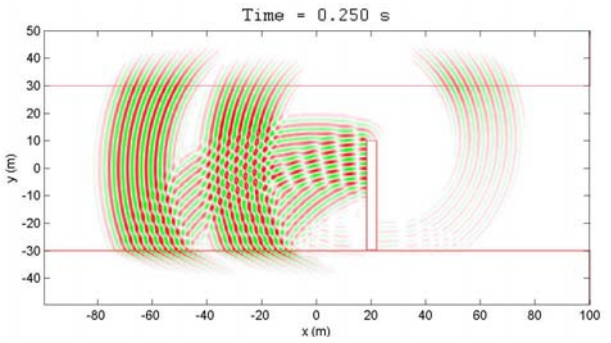

FIG. 10: Propagation above a soft porous ground in the presence of a rigid barrier, 0.250 s after source initiation.

$$Z(\omega) = \frac{\rho c q}{\Omega}\sqrt{\frac{1-i\omega\tau_z}{-i\omega\tau_z}}, \tag{8}$$

where $\tau_z = (\gamma/2)\,\tau_v$. This approximation is compared to (7) in Figure 11. Quite interestingly, one can show that (8) has the same functional form as an impedance derived from the low-frequency approximations (5) and (6). Physically, this suggests that the convolution terms in (3) and (4), which cause dissipation of propagating acoustic energy at higher frequencies, do not significanly affect the impedance. The inverse transform of Eq. (8) can be found in tables. It is

$$p(t) = \frac{\rho c q}{\Omega}\left\{ w_n(t) + \frac{1}{2\tau_z}\int_{-\infty}^{t}\left[I_1\left(\frac{t-t'}{2\tau_z}\right) + I_0\left(\frac{t-t'}{2\tau_z}\right)\right]\exp\left(-\frac{t-t'}{2\tau_z}\right) w_n(t')\, dt'\right\}, \tag{9}$$

where I_0 and I_1 are the modified Bessel functions of zeroth and first order, respectively.

The FDTD calculation for propagation with a barrier and soft porous ground from Section 3.1 is repeated in Figure 12, except that the ground interaction in this instance is calculated with Eq. (9). Although the propagation in the ground is not explicitly calculated, the appearance of the ground reflections is nearly the same as in Figure 10.

4. CONCLUSION

Improvements in acoustic FDTD techniques, and the increasing capabilities of modern parallel-processing computers, make possible highly detailed calculations of sound propagation through the atmosphere with real-world features such as complex reflecting surfaces, distributed moving sources, and dynamic turbulence fields. In this paper, we summarized recent efforts in developing a rigorous FDTD implementation of sound propagation in a moving, inhomogeneous fluid. As an illustration, calculations of low-frequency sound propagation through an atmospheric large-eddy simulation were presented. We have also succeeded in formulating and numerically implementing new

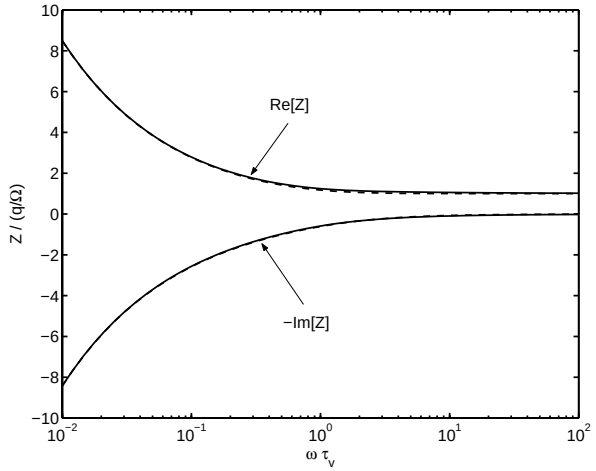

FIG. 11: Comparison of the exact impedance equation from the relaxation model Eq. (7) (solid lines) and its approximation Eq. (8) (dashed lines).

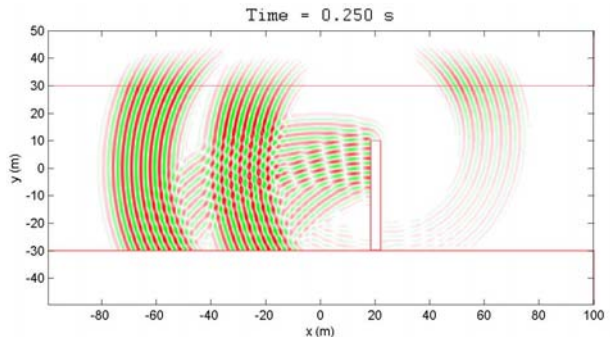

FIG. 12: Propagation above a soft porous ground in the presence of a rigid barrier, 0.250 s after source initiation. Calculation was performed with a time-domain boundary condition for the ground interface.

time-domain methods for handling sound interactions with the ground surface. The methods are unique in that they are based on full-frequency equations for sound propagation in porous materials including viscous and thermal diffusion processes.

Taken together, the progress reported here lays the foundation for highly realistic simulations of atmospheric sound propagation. Among the applications are virtual testing of tactical acoustic sensors and their associated information processing algorithms. We anticipate that this new capability, when applied to sensor design and procurement for the Army's Future Force, will substantially lower development costs and time cycles, and ultimately improve sensor performance in complex battlefield environments.

ACKNOWLEDGMENTS

Funding for this project was provided by the DoD High Performance Computing Modernization Office's Common High-Performance Scalable Software Initiative and the U.S. Army Engineer Research and Development Center. The large-eddy simulation data were provided by Edward Patton and Peter Sullivan of the National Center for Atmospheric Research. Sandia National Laboratories is operated by Sandia Corporation, a Lockheed Martin Company, for the USDOE under contract 94-AL85000.

REFERENCES

Berthelot, Y. H., 2001: Surface acoustic impedance and causality. *J. Acoust. Soc. Am.*, **109**, 1736–1739.

Botteldooren, D., 1994: Acoustical finite-difference time-domain simulation in a quasi-Cartesian grid. *J. Acoust. Soc. Am.*, **95**, 2313–2319.

Fellah, Z. E. A. and C. Depollier, 2000: Transient acoustic wave propagation in rigid porous media: a time-domain approach. *J. Acoust. Soc. Am.*, **107**, 683–688.

Graves, R. W., 1996: Simulating seismic wave propagation in 3D elastic media using staggered-grid finite differences. *Bull. Seismol. Soc. Am.*, **86**, 1091–1106.

Ostashev, V. E., 1997: *Acoustics in Moving Inhomogeneous Media*. E & FN Spon, London.

Ostashev, V. E., D. K. Wilson, L. Liu, D. F. Aldridge, N. P. Symons, and D. H. Marlin, 2004: Equations for finite-difference, time-domain simulation of sound propagation in moving media and numerical implementation. *J. Acoust. Soc. Am.* Submitted.

Salomons, E. M., 2001: *Computational Atmospheric Acoustics*. Kluwer, Dordrecht.

Salomons, E. M., R. Blumrich, and D. Heimann, 2002: Eulerian time-domain model for sound propagation over a finite-impedance ground surface. Comparison with frequency-domain models. *Acust. Acta Acust.*, **88**, 483–492.

Sullivan, P. P., J. C. McWilliams, and C.-H. Moeng, 1994: A subgrid-scale model for large-eddy simulation of planetary boundary-layer flows. *Boundary-Layer Meteorol.*, **71**, 247–276.

Symons, N., D. Aldridge, D. K. Wilson, D. Marlin, and V. Ostashev, 2003: 3D finite-difference simulation of acoustic waves in turbulent moving media. *J. Acoust. Soc. Am.*, **114**, 2440. Abstract only.

Wilson, D. K., 1993: Relaxation-matched modeling of propagation through porous media, including fractal pore structure. *J. Acoust. Soc. Am.*, **94**, 1136–1145.

Wilson, D. K. and L. Liu, 2004: Finite-difference, time-domain simulation of sound propagation in a dynamic atmosphere. Technical Report ERDC/CRREL TR-04-12, U.S. Army Cold Regions Research and Engineering Laboratory, 72 Lyme Rd, Hanover, NH 03755-1290.

Wilson, D. K., V. E. Ostashev, and S. L. Collier, 2004: Time-domain equations for sound propagation in rigid-frame porous media. *J. Acoust. Soc. Am.* Accepted.

Zwikker, C. and C. W. Kosten, 1949: *Sound Absorbing Materials*. Elsevier, New York.